JOURNAL OF PROPULSION AND POWER
Vol. 26, No. 4, July–August 2010

Hydroxyl-Tagging-Velocimetry Measurements of a Supersonic Flow over a Cavity

Michael D. Lahr,* Robert W. Pitz,† and Zachary W. Douglas‡
Vanderbilt University, Nashville, Tennessee 37235
and
Campbell D. Carter§
U.S. Air Force Research Laboratory, Wright-Patterson Air Force Base, Ohio 45433

DOI: 10.2514/1.47264

Hydroxyl-tagging-velocimetry measurements were made throughout the compressible flowfield of a Mach 2 air flow over a cavity. The supersonic flowfield simulates the pilot region of scramjet combustion under nonreacting conditions. In the hydroxyl-tagging-velocimetry method, ArF excimer laser (193 nm) beams pass through a humid gas flow, dissociating water to form a tagging grid of hydroxyl molecules. The hydroxyl-tagging-velocimetry grid density has been increased to 11 × 11 to yield up to 120 velocity vectors of the two-dimensional flow over a fixed time delay of 2–3 μs. Instantaneous single-shot measurements of two-dimensional flow patterns were made in the nonreacting Mach 2 flow over a wall cavity under low- and high-backpressure conditions. Single-shot profiles were analyzed to yield mean and rms deviation velocity profiles in the Mach 2 nonreacting flow. Compressibility greatly reduces the growth rate of the supersonic shear layer formed at the edge of the cavity. A set of velocity data (spanning the entire length of the cavity) for an open wall cavity in a supersonic flow under low- and high-backpressure conditions was compiled for validation of computational fluid dynamics models.

I. Introduction

ACCURATE nonintrusive velocimetry measurements are essential to validating computational fluid dynamics (CFD) codes for the development of scramjet-powered hypersonic flight vehicles. In scramjet flow paths, wall cavities are commonly used to stabilize the core-flow flame without excessive drag penalty [1,2]. They also provide a recirculation region with sufficient residence time for sustaining reaction and core-flow mass exchange. Velocity measurements are needed in this type of configuration under supersonic conditions for modeling and simulation purposes but require nonintrusive methods. Hot wire probes can easily produce flow disturbances in supersonic flows over cavities that lead to large velocity uncertainties [3]. Previously, particle-based velocity methods have been used to measure velocity in supersonic flows over a cavity. Samimy et al. [4] measured the velocity flowfield of a Mach 2.5 flow over a rectangular cavity/ramp with laser Doppler velocimetry (LDV). Zhang et al. [5] measured the velocity flowfield of a Mach 2 flow over a two-dimensional rectangular cavity with particle imaging velocimetry (PIV). Also, Ünalmis et al. reported PIV measurements for a limited region of a Mach 5 flow over a cavity [6]. In particle-based velocity methods, such as PIV, LDV, and planar Doppler velocimetry [7], laser radiation is scattered from tracer particles either inserted or naturally available in the flow. However, in supersonic flows, the tracer particles encounter shock waves and rapid accelerations leading to differences between the particle tracer velocity and the gas velocity due to particle drag and inertial effects [8]. Also, supersonic flows are generally studied in confined flows with optical windows that can be easily obscured by a coating of the tracer seed [9].

Laser-based molecular velocity methods directly measure the local gas velocity in the supersonic flow, negating the various problems posed by particle-based methods. In Doppler-shift methods that measure local velocity, the Doppler shift of radiation scattered from molecules (or atoms) is measured and related to velocity. In laser-induced fluorescence (LIF) methods, one records the Doppler shift of the LIF emission from gases, such as copper [10], hydroxyl [11,12], nitric oxide [13], sodium [14], and iodine [15]. Doppler-shift LIF methods are well suited to high-speed flows where the Doppler shift is much larger and more easily measured. However, the method normally provides only average flow velocities due to insufficient signal strength, and the addition of chemical species is often impractical in supersonic test facilities. Other Doppler-shift velocity methods are based on Rayleigh scattering of laser radiation from the gas molecules [16–18]. However, Rayleigh scattering can be orders of magnitude weaker than either LIF or particle scattering. In confined aerodynamics facilities, the Rayleigh scattering signals are difficult to differentiate from the much stronger laser scattering from tunnel walls and particles in the flow [19]. The velocity component measured by Doppler-shift methods (i.e., LIF or Rayleigh scattering) is defined by the geometry/orientation of the laser beam/sheet and the observer; in aerodynamic facilities with limited optical access, this can prevent measurement of the desired velocity feature [19].

Molecular tagging techniques allow measurement of the gas velocity by time-of-flight [19–41]; the technique is capable of measuring all three components of velocity using stereoscopic vision [28]. The molecules in the gas flow are tagged or marked with a laser; the movement of the tag with time gives the velocity. There are no particle lag or nonuniformity issues associated with molecular velocimetry. The tagged region is imaged by LIF or phosphorescence. This time-of-flight measurement of velocity can be easily implemented because it does not require the complex calibrations or corrections necessary in the Doppler-shift method. In some molecular tagging methods, gas molecules (or atoms) are seeded into the flow and subsequently tagged with a laser beam; the seeded

Presented as Paper 2006-40 at the 44th AIAA Aerospace Sciences Meeting and Exhibit, Reno, NV, 9–12 January 2006; received 18 September 2009; revision received 23 March 2010; accepted for publication 23 March 2010.

*Graduate Student, Department of Mechanical Engineering; currently Engineer, Brasfield and Gorrie, 200 Colonial Center Parkway, Lake Mary, Florida 32746.

†Professor, Department of Mechanical Engineering. Associate Fellow AIAA.

‡Undergraduate Student, Department of Mechanical Engineering; currently Engineer, Harris Corporation, Melbourne, Florida 32919.

§Principal Aerospace Engineer, Associate Fellow AIAA.

molecule can be electronically excited, vibrationally excited, ionized, or photodissociated to form a new molecule. Researchers have used a variety of molecular seeds in this technique, including acetone [20], biacetyl [21,22], nitric oxide [19,23,24], nitrogen dioxide [24,25], sodium [26], strontium [27], and tert–butyl nitrate [28]. Seeding a flow with molecules or atoms is often undesirable due to a variety of reasons (expense, seeding toxicity, corrosive behavior, etc.).

Unseeded molecular tagging methods use gas tags produced from molecules naturally occurring in air (i.e., nitrogen, oxygen, water vapor). These tags include N_2^+ ion [29], ozone [30–32], hydroxyl [32–37], nitric oxide [38–40], and vibrationally excited oxygen [17,41]. Furthermore, some of the tag methods use nonlinear laser excitation, such as Raman excitation plus laser-induced electronic fluorescence (RELIEF) [17,41], air photolysis and recombination tracking [38–40], and two-photon dissociation of H_2O [33]; these nonlinear techniques produce tags from air in a small region near the laser focus. Hydroxyl tagging velocimetry (HTV) is a linear method in which H_2O is photodissociated into H and OH in a single photon process; an ArF excimer laser operating at 193 nm is typically used for this purpose [32,35–37]. In atmospheric air, photodissociation by the ArF laser produces strong lines of OH ($\sim$100 ppm [37]) against a negligible OH background (less than 1 ppt). Hydroxyl is an optimal tag for supersonic flow, as OH is formed immediately by the pulsed ArF laser, and the OH has a sufficient lifetime (greater than 10 μs) to allow the measurement of the velocity by time of flight in the supersonic flow [37].

Nonintrusive velocity data is needed in flows relevant to scramjet combustion to better understand the complex flowfield around the pilot region and to advance CFD models [2,42]. An optically accessible supersonic flow facility has been developed to study cavity-stabilized supersonic nonreacting and reacting flows [2,43–45]. Previously, the HTV method was applied to measure the Mach 2 flow over a cavity, using a 7×7 grid to probe a limited portion of the cavity flowfield [46]. In this work, the HTV method is applied to the same Mach 2 flow over a wall cavity to obtain instantaneous two-dimensional velocity images, mean velocity profiles, and rms velocity profiles throughout the cavity flowfield.

II. Experimental System

HTV experiments were conducted at the supersonic flow facility in Research Cell 19 at the U.S. Air Force Research Laboratory in the Propulsion Directorate, Wright-Patterson Air Force Base. A schematic of the flow facility is shown in Fig. 1. The air supply to the wind tunnel consists of a series of compressors and a gas-fired heat exchanger to produce high-pressure high-temperature air at the desired test conditions. A two-dimensional nozzle produces a uniform, Mach 2 stream (51 mm high by 153 mm wide) that is followed by a constant-area section that is 178 mm in length. Immediately downstream of the constant-area section, the test section begins and the bottom wall diverges at an angle of 2.5°. The wall cavity is formed 76 mm from the end of the constant-area section. Figure 2 shows a schematic of the wall cavity (the flow is left to right). The wall cavity (16.5 mm deep, 66 mm long, and 153 mm wide) provides a flame pilot region where fuel is added for study

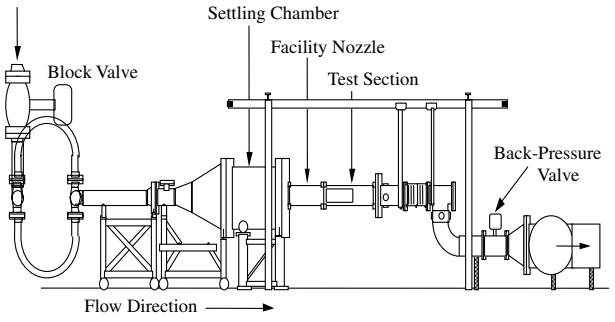

Fig. 1 Facility schematic of the supersonic combustion tunnel in Research Cell 19.

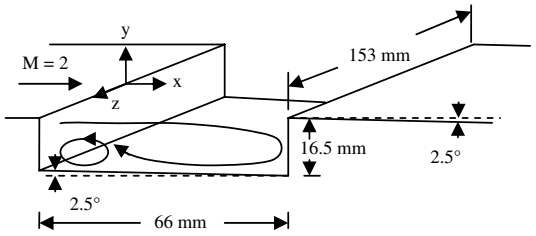

Fig. 2 Schematic of the Mach 2 flow over a cavity.

under reacting conditions [2,44,45]. A shear layer forms at the edge of the first step in the cavity, and a recirculation zone is produced by the cavity. This is an open cavity, since the cavity length (L) to depth (D) ratio is $L/D = 4$. For $L/D < 7$–10, the cavity is open, and the shear layer reattaches to the back face of the cavity, leading to reduced pressure loss when compared with closed cavities ($L/D > 7$–10) where the shear layer attaches to the cavity lower wall [1].

The HTV measurements were taken in the wall cavity of the test section. A schematic of the HTV system is shown in Fig. 3. Air entered the test section at Mach 2 with a flow rate of approximately 1.4 kg/s. A Lambda Physik COMPex 150T ArF excimer laser was used to produce 193 nm radiation. The ArF excimer laser beams were directed through the tunnel windows to create a grid providing the greatest number of visible crossing points while minimizing laser scatter. Three different configurations were used to move the grid downstream of the leading edge of the cavity in discrete intervals; however, only the position of the grid optics had to be altered to allow for this progression. The basis for the setup, as shown in Fig. 3, consists of the ArF excimer laser beam (20 mm high by 10 mm wide, 150 mJ/pulse, broadband, and 1 nm bandwidth) being split into two beams by a beam splitter: one traveling under the test section to the other side, and the other beam remaining on the same side of the configuration. This provided adequate crossing angles for the written lines in the flow regime across the cavity. Each of the laser beams is sent through the new grid-forming optics to produce two sets of 11 beams each. The grid optics consist of two major components placed very close together: a 300 mm focal length cylindrical lens (25×40 mm) and a stack of 11 cylindrical lenses (300 mm fl, 20 mm wide by 2 mm high). The beam diameter was about 0.3 mm in the measurement zone. The energies for the two sets of beams before transmission into the tunnel were as low as 9.4 mJ/pulse on the excimer laser side with a path length of 2.8 m and 7.4 mJ/pulse on the dye laser side with a path length of 3.9 m.

The ArF excimer generated an 11×11 grid of OH lines that was subsequently imaged by LIF using the overlapped $Q_1(1) + R_2(3)$ transition of the $A^2\Sigma^+(v' = 1) \leftarrow X^2\Pi_i(v'' = 0)$ band at 282 nm. A Spectra Physics model GRC 170 neodymium-doped yttrium aluminum garnet (Nd:YAG) laser pumped a Lumonics HD-300 Hyperdye dye laser. The output of the dye laser was doubled by an

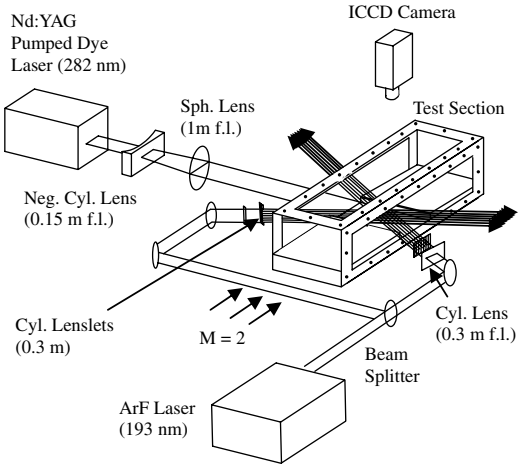

Fig. 3 Schematic of the HTV experimental system.

Table 1 Flow conditions for a Mach 2 flow with a wall cavity

Test	Stagnation conditions		Isentropic conditions, Mach 2		Air mass flow rate, kg/s	Backpressure valve, %	Cavity bottom-wall pressure, kPa	Downstream bottom-wall pressure, kPa[a]
	P_o, kPa	T_o, K	P, KPa	T, K				
A	170	520	22	290	1.4	0	25	15
B	170	520	22	290	1.4	60	25	54

[a]Bottom-wall pressure 200 mm downstream of the end of the cavity.

Inrad Autotracker II to produce about 20 mJ/pulse of 282 nm laser radiation. A small portion of the 282 nm beam was split off and directed over a small flame and then to a photodiode. Signals from the photodiode and a photomultiplier tube (recording the OH LIF from the flame) were displayed on an oscilloscope to ensure proper operation of the dye laser and good overlap with the OH transition. Timing of the lasers and camera was accomplished with a Quantum Composer (model 9318E) pulse generator. The random (shot-to-shot) timing error between the lasers was evaluated from a collection of 200 oscilloscope photodiode traces (showing the timing of the two laser pulses); the standard deviation for the relative timing was about ± 8 ns, thus the magnitude of the error was less than 0.5% of the typical 2 μs timing separation.

The 282 nm beam (5 ns pulse duration) was expanded by a -150 mm focal-length cylindrical lens and focused by a 1000 mm focal-length spherical lens to form a $\sim$40 mm-wide sheet to image the grid. The 282 nm sheet was retroreflected back through the tunnel to improve signal strength; the delay between the forward and backward laser sheet was about 5 ns. Both the OH-probe laser sheet and the 193 nm grid were rotated parallel to the tunnel bottom floor at an angle of 2.5° off the horizontal plane.

A PI-MAX Superblue intensified CCD camera was used to record the fluorescence from the created OH. The camera was fitted with a 45 mm f/1.8 UV Cerco lens, and Schott glass filters (WG-305 and UG-5) were employed to block background scattering and fluorescence from tunnel surfaces. With the camera looking down through the top window of the test section, the field of view was 40 mm square. The 512×512 pixel array of the PI-MAX camera was binned 2×2 to improve signal strength, and each 2×2 binned pixel viewed a 156×156 μm region of the flowfield.

A three-dimensional traversing table was located beneath the tunnel. Focusing optics for the setup and the intensified charge-coupled device (ICCD) camera were arranged and mounted on the table to allow the laser grid and sheet height location to be varied. The velocity trends above and in the cavity could then be probed.

III. Results

HTV measurements were made in nonreacting Mach 2 flow with an 11×11 grid pattern. As shown in Table 1, both tests had the same stagnation conditions (170 kPa, 520 K) leading to isentropic conditions at Mach 2 of 22 kPa and 290 K. Test A is a low-backpressure condition with the backpressure valve fully open downstream of the test section; 200 mm downstream of the end of cavity, the bottom-wall static pressure is 15 kPa and is below the Mach 2 isentropic static pressure of 22 kPa. Under low-backpressure conditions, the tunnel flow above the cavity is basically free of shock waves, with only a few weak oblique shocks anchored to the leading edge, as shown in Fig. 4. Test B is a high-backpressure condition, with the backpressure valve 60% closed to simulate the pressure rise from main-duct combustion; 200 mm downstream of the end of the cavity, the bottom-wall pressure is 54 kPa and is above the Mach 2 isentropic static pressure of 22 kPa. With the backpressure valve partly closed (creating high backpressure), strong shocks appear above the cavity, causing the shear layer to be deflected upward (see Fig. 2 of [44]). Both tests had the same cavity bottom-wall pressure: 25 kPa. The two tests were conducted to explore the velocity trends in the test section, with and without shock waves present in the cavity flow.

The wind-tunnel compressor facility supplied dry air with inadequate humidity levels to achieve strong OH signals in the test section. Water was sprayed into the stagnation chamber at flow rates of 17–25 g/s to achieve a relative humidity up to 32% in the test section that gave adequate OH signals while avoiding water condensation in the test section. Velocities were recorded along the streamwise length of the cavity, with measurements taken vertically at each location. Six overlapping regions were analyzed, where the total measurement zone is shown in the shaded region seen in Fig. 5. Examples of two-dimensional velocity images using the HTV method with the 11×11 grid are shown in Figs. 6–9. The location of the velocity images are given with respect to the coordinate system shown in Fig. 2. Figure 6 is an averaged HTV image (100 single shots) used as a reference for the displaced grid patterns. Figures 7–9 are analyzed HTV images with velocity vectors shown on top of displaced 11×11 HTV grid patterns. The vector field is obtained by a spatial correlation method described by Gendrich and Koochesfahani [47]; this method was used previously for the 7×7 HTV grid measurements [46]. Figures 7–9 include both irregular grid and regular grid spacing for the vector representation; the irregular

Fig. 4 Shadowgraph single-shot image over a rectangular cavity in a Mach 2 nonreacting cavity flow at low-backpressure conditions [45].

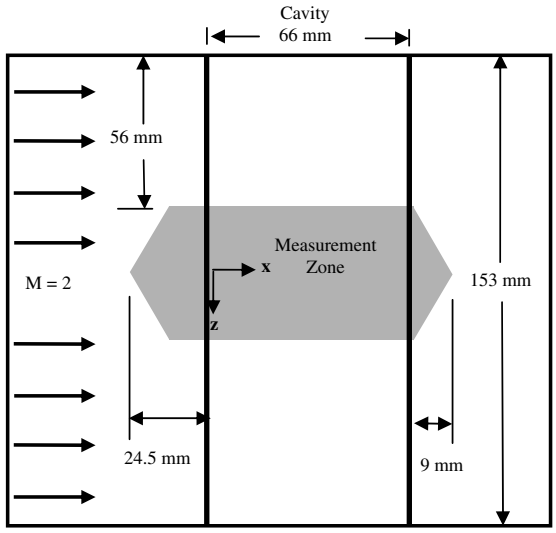

Fig. 5 Overhead schematic of the cavity, showing the position of the HTV images relative to the cavity steps and test-section walls.

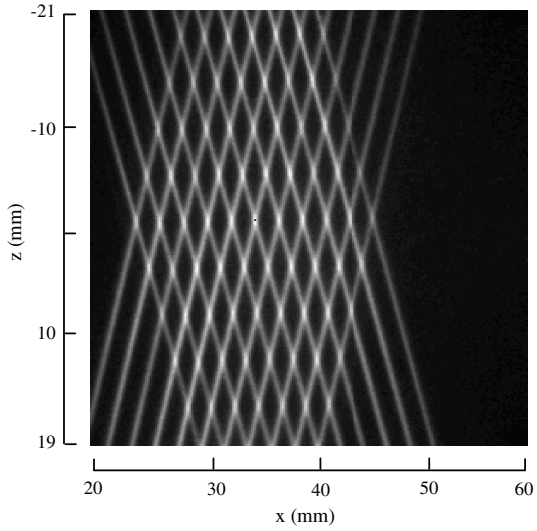

Fig. 6 Averaged undelayed HTV image (at $y = 15.62$ mm, where $z = 0$ is the centerline of the cavity, and $x = 0$ is at the front face of the cavity).

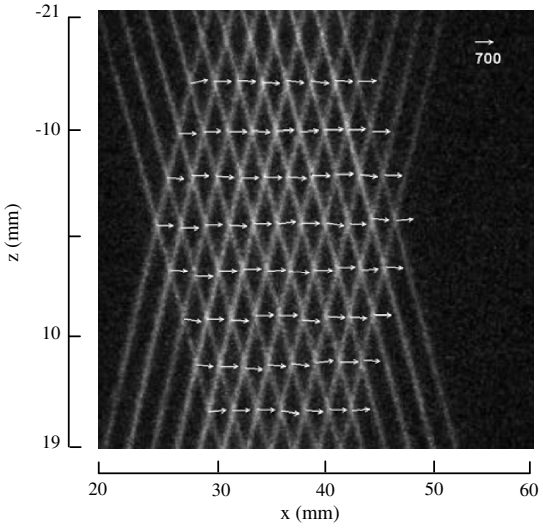

a)

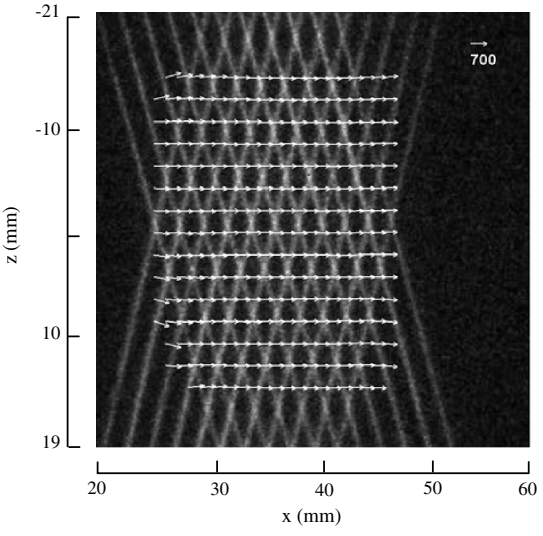

b)

Fig. 7 Single-shot HTV images, giving velocity images with a) irregular and b) regular grids in a Mach 2 nonreacting scramjet cavity flow for the low-backpressure case (at $y = 15.62$ mm, where $z = 0$ is the centerline of the cavity, and $x = 0$ is at the front face of the cavity).

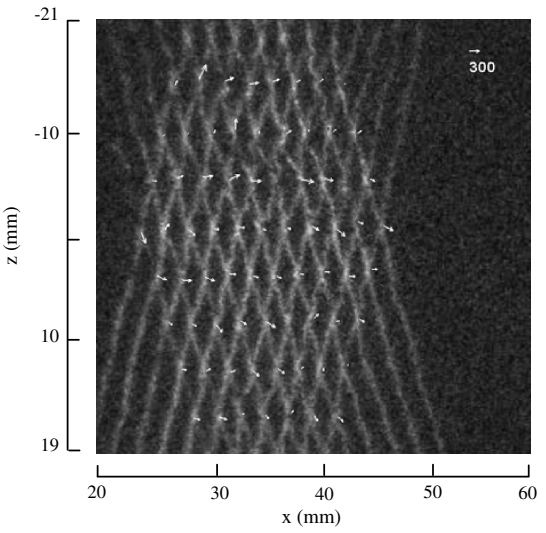

a)

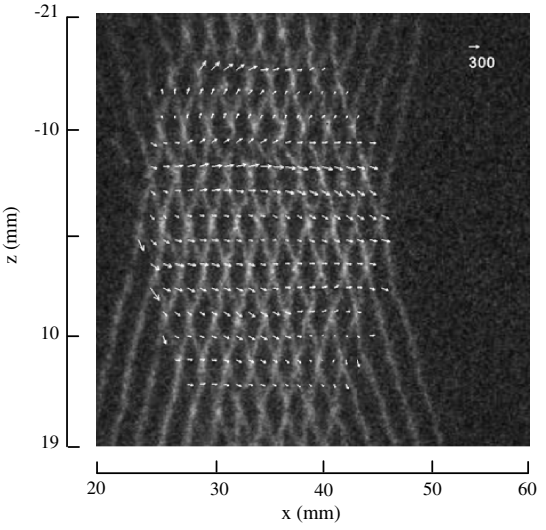

b)

Fig. 8 Single-shot HTV images, giving velocity images with a) irregular and b) regular grids in a Mach 2 nonreacting scramjet cavity flow for the low-backpressure case (at $y = 0.41$ mm, where $z = 0$ is the centerline of the cavity, and $x = 0$ is at the front face of the cavity).

grid patterns from the HTV images shown in Figs. 7a, 8a, and 9a are mapped onto regular grids shown in Figs. 7b, 8b, and 9b. The mapping procedure and its performance are described by Cohn and Koochesfahani [48]. The time delays varied in these experiments from 1 to 3 μs, with the delay at 2 μs for all freestream measurements.

In the freestream above the cavity, the velocity pattern shown in Fig. 7 is very uniform, with a value of about 680 m/s (note the reference vector of 700 m/s). Moving down into the shear layer, the flow becomes much less uniform and exhibits a decrease in velocity to about 175 m/s (note the reference vector of 300 m/s), as seen in Fig. 8. A single-shot image of flow in the cavity is shown in Fig. 9. At this depth, the flow reverses, with the negative velocity reaching up to 200 m/s (note the reference vector of 200 m/s).

The average signal-to-noise ratio (SNR) of the single-shot images ranges from 5 to 11. With crossing angles between 135 and 150° at this SNR range, the total displacement of the line crossings can be determined within 0.1 pixel, or a displacement uncertainty of ± 16 μm according to previous calculations (see Fig. 5 of [47]).[¶]

[¶]Gendrich and Koochesfahani [47] give errors in 95% confidence intervals that are a factor of two larger than standard deviation intervals.

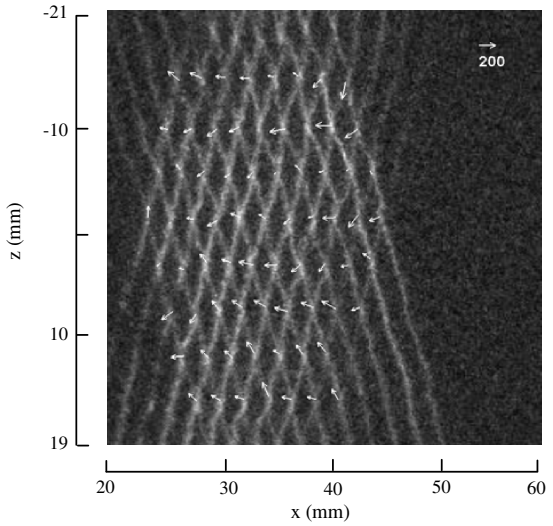

a)

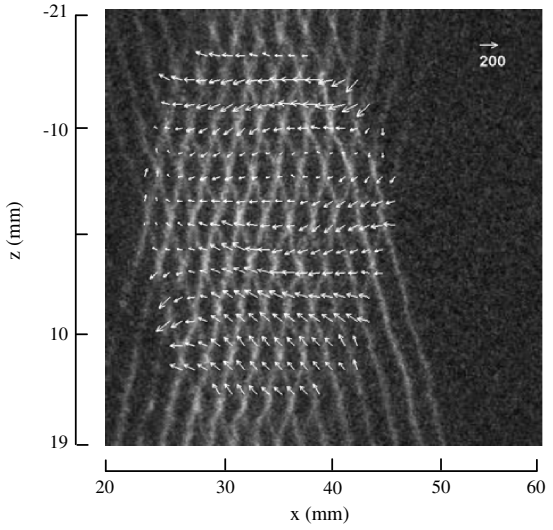

b)

Fig. 9 Single-shot HTV images, giving velocity images with a) irregular and regular b) grids in a Mach 2 nonreacting scramjet cavity flow for the low-backpressure case (at $y = -9.75$ mm, where $z = 0$ is the centerline of the cavity, and $x = 0$ is at the front face of the cavity).

While the total displacement can be determined to 0.1 pixel, because of the elongated cross section of the crossing points in the z direction, the uncertainty in the z-direction displacement is five times greater than the uncertainty in the x-direction displacement (see Fig. 6 of [47]). For a 2 μs delay, the uncertainty due to the characteristics of the crossing points is, therefore, ± 8 m/s for the total velocity. Thus,

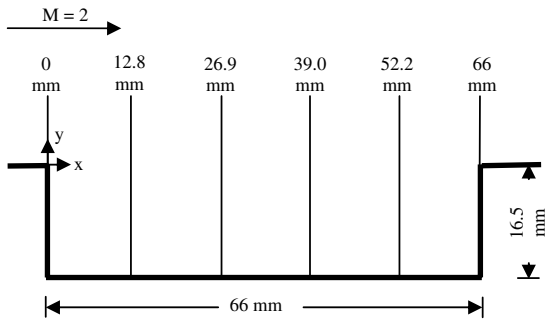

Fig. 10 Sideview schematic of the cavity, showing the profile locations along the x axis.

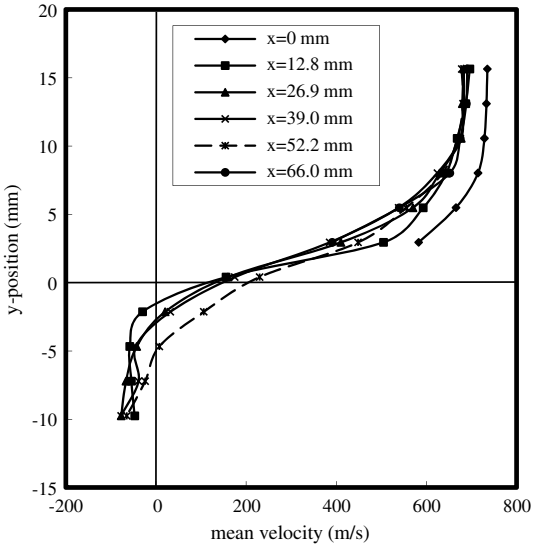

Fig. 11 Streamwise mean velocity profiles in the Mach 2 cavity flow, showing shear layer between the freestream and the cavity at low-backpressure conditions ($z = 0$ mm, where $z = 0$ is the centerline of the cavity, and $x = 0$ is at the front face of the cavity).

for full-scale displacement, as seen in the freestream, a relative uncertainty of $\pm 1\%$ can be achieved in the streamwise direction.

Mean velocity and rms deviation velocity profiles were obtained by analyzing instantaneous velocity images (100 single shots at each data point) at various streamwise locations (x axis) in the cavity, as shown in Fig. 10. Streamwise mean and rms velocity profiles are shown in Figs. 11 and 12 and are taken near the centerline of the tunnel, from the freestream to down in the cavity. In Fig. 11, the average velocities above the cavity range from about 680 to 730 m/s. At the freestream inlet, the velocity is 730 m/s; this is higher than the expected value of 680 m/s for the Mach 2 nozzle, due to the bottom-wall divergence. The velocity drop in the freestream is caused by the oblique shock anchored to the leading edge (seen in Fig. 4). The average velocity decreases in the shear layer and becomes negative (about -75 m/s) in the cavity. The shear layer profile and recirculation zone appear to be similar to a subsonic flow formed behind a rearward-facing step [49], except the shear layer growth rate is greatly reduced in the compressible flow. The vorticity thickness δ_ω of the shear layer is given by

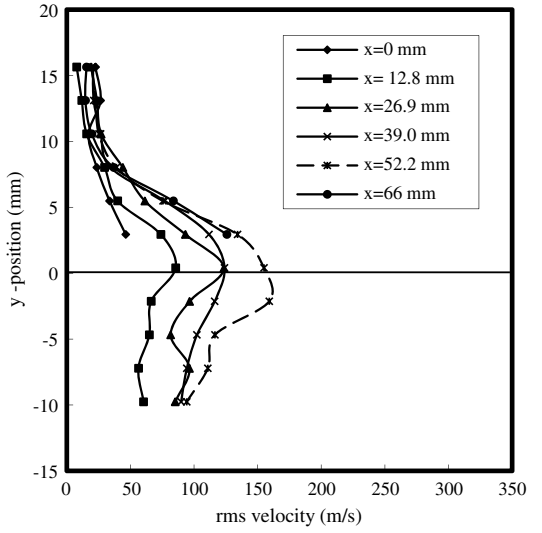

Fig. 12 Streamwise rms velocity profiles in the Mach 2 cavity flow, showing shear layer between the freestream and the cavity at low-backpressure conditions ($z = 0$ mm, where $z = 0$ is the centerline of the cavity, and $x = 0$ is at the front face the cavity).

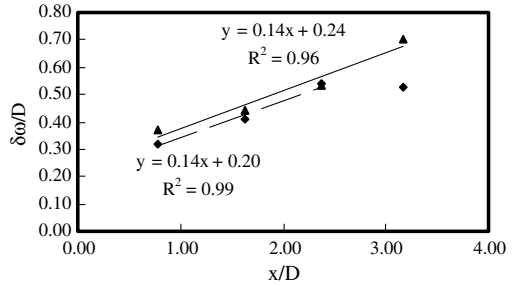

Fig. 13 Vorticity thickness of the compressible shear layer under low- and high-backpressure conditions, showing a growth rate of $\delta'_\omega = 0.14$. [◆: low pressure, ▲: high pressure, dashes: linear (low pressure), line: linear (high pressure)].

$$\delta_\omega = \Delta U \Big/ \left.\frac{\partial u}{\partial y}\right|_{\max} \tag{1}$$

From the velocity profiles shown in Fig. 11, the shear layer vorticity thickness δ_ω is estimated and plotted versus downstream distance (x/D) for the low pressure shear layer in Fig. 13. For the initial shear layer $(x/D < 3)$, the shear layer growth rate is

$$\delta'_\omega \cong 0.14 \tag{2}$$

which is half the value found for a subsonic shear layer formed at a backward-facing step ($\delta'_\omega = 0.28$ [49]). Here, the convective Mach number is $\sim$1, and a reduction in shear layer growth of at least 50% is expected from compressibility effects [50].

The rms deviation velocities for the low-backpressure case are shown in Fig. 12. The rms values in the freestream are as low as 8 m/s, or about 1.2%. This rms value is due to a combination of freestream turbulence and measurement precision. Recall that the displacement error is $\sim$1%, and the timing error is less than 0.5% of the typical 2 μs delay. The rms values increase in the shear layer and then decrease slightly in the cavity, similar to what is observed in a subsonic flow behind a rearward-facing step [49].

The mean velocity and rms deviation velocity profiles for the high-backpressure case are shown in Figs. 14 and 15. The profiles are somewhat different from those for the low-backpressure case. Unsteady shock waves previously observed above the cavity (see Fig. 2 of [44]) alter the mean and rms velocity profiles. The compressible shear layer is deflected upward, leading to slightly

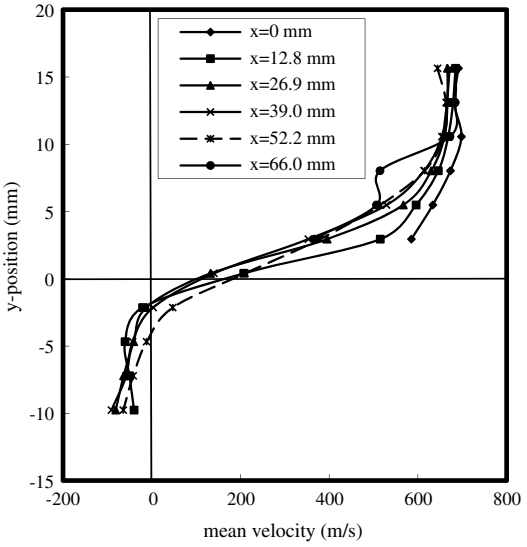

Fig. 14 Streamwise mean velocity profiles in the Mach 2 cavity flow, showing shear layer between the freestream and the cavity at high-backpressure conditions ($z = 0$ mm, where $z = 0$ is the centerline of the cavity, and $x = 0$ is at the front face of the cavity).

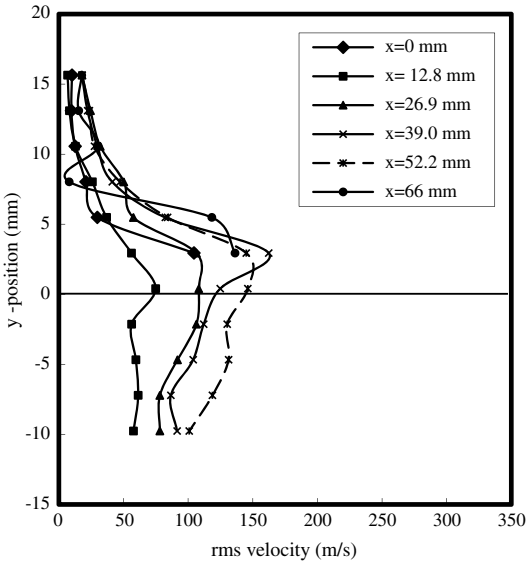

Fig. 15 Streamwise rms velocity profiles in the Mach 2 cavity flow, showing shear layer between the freestream and the cavity under high-backpressure conditions ($z = 0$ mm, where $z = 0$ is the centerline of the cavity, and $x = 0$ is at the front face of the cavity).

reduced mean velocities and rms deviation velocities that peak above the cavity. As seen in Fig. 13, the growth rate of the compressible shear layer under both low- and high-backpressure conditions is essentially the same value ($\delta'_\omega = 0.14$). However, in the high-backpressure case, the growth rate is maintained for a distance that nearly spans the entire cavity length.

IV. Conclusions

Previously using a 7×7 grid pattern, nonintrusive measurements of velocity were obtained in a Mach 2 flow with a wall cavity, using HTV in one centralized location. In this work, an 11×11 grid pattern allowed the measurement of up to 120 vectors in the flowfield, and velocity measurements are obtained from edge to edge in the Mach 2 nonreacting flow over the cavity under low- and high-backpressure conditions. The velocity measurements are accurate to ± 8 m/s, or $\pm 1\%$ of the freestream velocity of 730 m/s. The instantaneous planar measurements are analyzed to determine the mean and rms deviation velocities in the streamwise direction. Under both low- and high-backpressure conditions, the growth rate of the compressible shear layer formed at the edge of the cavity is the same, but the value is half that of a subsonic shear layer formed at a backward-facing step. Under high-backpressure conditions, the compressible shear layer is deflected upward, leading to rms deviation velocities that peak above the top of the cavity. These measurements demonstrate the benefits of HTV in comparison with particle-based methods that have difficulty in recirculation regions bordered by high-speed flows. Future work will explore, in detail, approaches to making measurements in reacting cavities with high-speed cross flows.

Acknowledgments

This research was supported by the U.S. Air Force Office of Scientific Research (AFOSR) Combustion and Diagnostics Program (Julian Tishkoff, Manager). M. D. Lahr and Z. W. Douglas were supported by the Propulsion Directorate's Summer Fellowship. R. W. Pitz was supported by an AFOSR summer faculty fellowship and the Arnold Engineering Development Center under contract No. F40600-03-D-0001. The authors also thank S. Pouya and M. Koochesfahani from Michigan State University for their help in analyzing the hydroxyl-tagging-velocimetry data and W. Terry and D. Schommer at Wright-Patterson Air Force Base for their technical support.

References

[1] Ben-Yakar, A., and Hanson, R. K., "Cavity Flame-Holders for Ignition and Flame Stabilization in Scramjets: An Overview," *Journal of Propulsion and Power*, Vol. 17, No. 4, 2001, pp. 869–877. doi:10.2514/2.5818

[2] Gruber, M. R., Baurle, R. A., Mathur, T., and Hsu, K.-Y., "Fundamental Studies of Cavity-Based Flameholder Concepts for Supersonic Combustors," *Journal of Propulsion and Power*, Vol. 17, No. 1, 2001, pp. 146–153. doi:10.2514/2.5720

[3] Settles, G. S., Williams, D. R., Baca, B. K., and Bogdonoff, S. M., "Reattachment of a Compressible Turbulent Free Shear Layer," *AIAA Journal*, Vol. 20, No. 1, 1982, pp. 60–67. doi:10.2514/3.51047

[4] Samimy, M., Petrie, H. L., and Addy, A. L., "A Study of Compressible Turbulent Reattaching Free Shear Layers," *AIAA Journal*, Vol. 24, No. 2, 1986, pp. 261–267. doi:10.2514/3.9254

[5] Zhang, N., Alvi, F. S., Alkislar, M. B., and Shih, C., "Supersonic Cavity Flows and Their Control," *AIAA Journal*, Vol. 44, No. 9, 2006, pp. 2118–2128. doi:10.2514/1.14879

[6] Ünalmis, Ö. H., Clemens, N. T., and Dolling, D. S., "Experimental Study of Shear-Layer/Acoustics Coupling in a Mach 5 Cavity Flow," *AIAA Journal*, Vol. 39, No. 2, 2001, pp. 242–252. doi:10.2514/2.1319

[7] Samimy, M., and Wernet, M. P., "Review of Planar Multiple-Component Velocimetry in High-Speed Flows," *AIAA Journal*, Vol. 38, No. 4, 2000, pp. 553–574. doi:10.2514/2.1004

[8] Koike, S., Takahashi, H., Tanaka, K., Hirota, M., Takita, K., and Masuya, G., "Correction Method for Particle Imaging Data Based on the Stokes Drag Law," *AIAA Journal*, Vol. 45, No. 11, 2007, pp. 2770–2777. doi:10.2514/1.30962

[9] Santoro, R. J., Pal, S., Woodward, R. D., and Schaaf, L., "Rocket Testing at University Facilities," AIAA Paper 2001-0748, Jan. 2001.

[10] Marinelli, W. J., Kessler, W. J., Allen, M. G., Davis, S. J., Arepalli, S., and Scott, C. D., "Copper Atom Based Measurements of Velocity in Turbulence and in Arc Jet Flows," AIAA Paper 91-0358, Jan. 1991.

[11] Allen, M., Davis, S., Kessler, W., Legner, H., McManus, K., Mulhall, P., Parker, T., and Sonnenfroh, D., "Velocity Field Imaging in Supersonic Reacting Flows Near Atmospheric Pressure," *AIAA Journal*, Vol. 32, No. 8, 1994, pp. 1676–1682. doi:10.2514/3.12159

[12] Klavuhn, K. G., Gauba, G., and McDaniel, J. C., "OH Laser-Induced Fluorescence Velocimetry Technique for Steady, High-Speed, Reacting Flows," *Journal of Propulsion and Power*, Vol. 10, No. 6, 1994, pp. 787–797. doi:10.2514/3.23816

[13] Paul, P. H., Lee, M. P., and Hanson, R. K., "Molecular Velocity Imaging of Supersonic Flows Using Pulsed Planar Laser-Induced Fluorescence of NO," *Optics Letters*, Vol. 14, No. 9, 1989, pp. 417–419. doi:10.1364/OL.14.000417

[14] Zimmerman, M., and Miles, R. B., "Hypersonic-Helium-Flowfield Measurements with Resonant Doppler Velocimeter," *Applied Physics Letters*, Vol. 37, No. 10, 1980, pp. 885–887. doi:10.1063/1.91784

[15] McDaniel, J. C., Hiller, B., and Hanson, R. K., "Simultaneous Multiple-Point Velocity Measurements Using Laser-Induced Iodine Fluorescence," *Optics Letters*, Vol. 8, No. 1, 1983, pp. 51–53. doi:10.1364/OL.8.000051

[16] Seasholtz, R. G., Zupanc, F. J., and Schneider, S. J., "Spectrally Resolved Rayleigh Scattering Diagnostic for Hydrogen-Oxygen Rocket Plume Studies," *Journal of Propulsion and Power*, Vol. 8, No. 5, 1992, pp. 935–942. doi:10.2514/3.23575

[17] Miles, R. B., and Lempert, W. R., "Quantitative Flow Visualization in Unseeded Flows," *Annual Review of Fluid Mechanics*, Vol. 29, No. 1, 1997, pp. 285–326. doi:10.1146/annurev.fluid.29.1.285

[18] Bivolaru, D., Cutler, A. D., Danehy, P. M., Gaffney, R. L., and Baurle, R. A., "Spatially and Temporally Resolved Measurements of Velocity in a H_2-Air Combustion-Heated Supersonic Jet," AIAA Paper 2009-0027, Jan. 2009.

[19] Houwing, A. F. P., Smith, D. R., Fox, J. S., Danehy, P. M., and Mudford, N. R., "Laminar Boundary Layer Separation at a Fin-Body Junction in a Hypersonic Flow," *Shock Waves*, Vol. 11, No. 1, 2001, pp. 31–42. doi:10.1007/PL00004055

[20] Lempert, W. R., Jiang, N., Sethuram, S., and Samimy, M., "Molecular Tagging Velocimetry Measurements in Supersonic Microjets," *AIAA Journal*, Vol. 40, No. 6, 2002, pp. 1065–1070. doi:10.2514/2.1789

[21] Hiller, B., Booman, R. A., Hassa, C., and Hanson, R. K., "Velocity Visualization in Gas Flows Using Laser-Induced-Fluorescence of Biacetyl," *Review of Scientific Instruments*, Vol. 55, No. 12, 1984, 1964–1967. doi:10.1063/1.1137687

[22] Stier, B., and Koochesfahani, N. M., "Molecular Tagging Velocimetry (MTV) Measurements in Gas Phase Flows," *Experiments in Fluids*, Vol. 26, No. 4, 1999, pp. 297–304. doi:10.1007/s003480050292

[23] Danehy, P. M., O'Byrne, S., Houwing, A. F. P., Fox, J. S., and Smith, D. R., "Flow-Tagging Velocimetry For Hypersonic Flows Using Fluorescence of Nitric Oxide," *AIAA Journal*, Vol. 41, No. 2, 2003, pp. 263–271. doi:10.2514/2.1939

[24] Hsu, A. G., Srinivasan, R., Bowersox, R. D. W., and North, S. W., "Two-Component Molecular Tagging Velocimetry Utilizing NO Fluorescence Lifetime and NO_2 Photodissociation Techniques in an Underexpanded Jet Flowfield," *Applied Optics*, Vol. 48, No. 22, 2009, pp. 4414–4423. doi:10.1364/AO.48.004414

[25] Orlemann, C., Schulz, C., and Wolfrum, J., "NO-Flow Tagging by Photodissociation of NO_2. A New Approach for Measuring Small-Scale Flow Structures," *Chemical Physics Letters*, Vol. 307, Nos. 1—2, 1999, pp. 15–20. doi:10.1016/S0009-2614(99)00512-6

[26] Barker, P., Thomas, A., Rubinsztein-Dunlop, H., and Ljungberg, P., "Velocity Measurements By Flow Tagging Employing Laser Enhanced Ionisation and Laser Induced Fluorescence," *Spectrochimica Acta, Part B (Atomic Spectroscopy)*, Vol. 50, No. 11, 1995, pp. 1301–1310. doi:10.1016/0584-8547(95)01353-X

[27] Rubinsztein-Dunlop, H., Littleton, B., Barker, P., Ljungberg, P., and Malmsten, Y., "Ionic Strontium Fluorescence as a Method of Flow Tagging Velocimetry," *Experiments in Fluids*, Vol. 30, No. 1, 2001, pp. 36–42. doi:10.1007/s003480000132

[28] Krüger, S., and Grünefeld, G., "Stereoscopic Flow-Tagging Velocimetry," *Applied Physics B (Lasers and Optics)*, Vol. 69, Nos. 5–6, 1999, pp. 509–512. doi:10.1007/s003400050844

[29] Ress, J. M., Laufer, G., and Krauss, R. H., "Laser Ion Time-of-Flight Velocity Measurements Using N_2^+ Tracers," *AIAA Journal*, Vol. 33, No. 2, 1995, pp. 296–301. doi:10.2514/3.12417

[30] Pitz, R. W., Brown, T. M., Nandula, S. P., Skaggs, P. A., DeBarber, P. A., Brown, M. S., and Segall, J., "Unseeded Velocity Measurement by Ozone Tagging Velocimetry," *Optics Letters*, Vol. 21, No. 10, 1996, pp. 755–757. doi:10.1364/OL.21.000755

[31] Ribarov, L. A., Wehrmeyer, J. A., Batliwala, F., Pitz, R. W., and DeBarber, P. A., "Ozone Tagging Velocimetry Using Narrowband Excimer Lasers," *AIAA Journal*, Vol. 37, No. 6, 1999, pp. 708–714. doi:10.2514/2.799

[32] Pitz, R. W., Wehrmeyer, J. A., Ribarov, L. A., Oguss, D. A., Batliwala, F., DeBarber, P. A., Deusch, S., and Dimotakis, P. E., "Unseeded Molecular Flow Tagging in Cold and Hot Flows Using Ozone and Hydroxyl Tagging Velocimetry," *Measurement Science and Technology*, Vol. 11, No. 9, 2000, pp. 1259–1271. doi:10.1088/0957-0233/11/9/303

[33] Boedeker, L. R., "Velocity Measurement by H_2O Photolysis and Laser-Induced Fluorescence of OH," *Optics Letters*, Vol. 14, No. 10, 1989, pp. 473–475. doi:10.1364/OL.14.000473

[34] Davidson, D. F., Chang, A. Y., DiRosa, M. D., and Hanson, R. K., "Continuous Wave Laser Absorption Techniques for Gasdynamic Measurements in Supersonic Flows," *Applied Optics*, Vol. 30, No. 18, 1991, pp. 2598–2608. doi:10.1364/AO.30.002598

[35] Wehrmeyer, J. A., Ribarov, L. A., Oguss, D. A., and Pitz, R. W., "Flame Flow Tagging Velocimetry with 193 nm H_2O Photodissociation," *Applied Optics*, Vol. 38, No. 33, 1999, pp. 6912–6917. doi:10.1364/AO.38.006912

[36] Ribarov, L. A., Wehrmeyer, J. A., Pitz, R. W., and Yetter, R. A., "Hydroxyl Tagging Velocimetry (HTV) in Experimental Airflows," *Applied Physics B (Lasers and Optics)*, Vol. 74, No. 2, 2002,

pp. 175–183.
doi:10.1007/s003400100777
[37] Ribarov, L. A., Wehrmeyer, J. A., Hu, S., and Pitz, R. W., "Multiline Hydroxyl Tagging Velocimetry Measurements in Reacting and Nonreacting Experimental Flows," *Experiments in Fluids*, Vol. 37, 2004, pp. 65–74.
doi:10.1007/s003400100777
[38] Dam, N. J., Klein-Douwel, J. H., Sijtsema, N. M., and ter Meulen, J. J., "Nitric Oxide Flow Tagging in Unseeded Air," *Optics Letters*, Vol. 26, No. 1, 2001, pp. 36–38.
doi:10.1364/OL.26.000036
[39] Sijtsema, N. M., Dam, N. J., Klein-Douwel, J. H., and ter Meulen, J. J., "Air Photolysis and Recombination Tracking: A New Molecular Tagging Velocimetry Scheme," *AIAA Journal*, Vol. 40, No. 6, 2002, pp. 1061–1064.
doi:10.2514/2.1788
[40] van der Laan, W. P. N., Tolboon, R. A. L., Dam, N. J., and ter Meulen, J. J., "Molecular Tagging Velocimetry in the Wake of an Object in Supersonic Flow," *Experiments in Fluids*, Vol. 34, 2003, pp. 531–533.
doi:10.1007/s00348-003-0593-1
[41] Noullez, A., Wallace, G., Lempert, W. R., Miles, R. B., and Frisch, U., "Transverse Velocity Increments In Turbulent Flow Using the RELIEF Technique," *Journal of Fluid Mechanics*, Vol. 339, 1997, pp. 287–307.
doi:10.1017/S0022112097005338
[42] Rizzetta, D. P., and Visbal, M. R., "Large-Eddy Simulation of Supersonic Cavity Flowfields Including Flow Control," *AIAA Journal*, Vol. 41, No. 8, 2003, pp. 1452–1462.
doi:10.2514/2.2128
[43] Gruber, M. R., and Nejad, A. S., "New Supersonic Combustion Research Facility," *Journal of Propulsion and Power*, Vol. 11, No. 5, 1995, pp. 1080–1083.
doi:10.2514/3.23940
[44] Gruber, M. R., Donbar, J. M., Carter, C. D., and Hsu, K.-Y., "Mixing and Combustion Studies Using Cavity-Based Flameholders in a Supersonic Flow," *Journal of Propulsion and Power*, Vol. 20, No. 5, 2004, pp. 769–778.
doi:10.2514/1.5360
[45] Rasmussen, C. C., Driscoll, J. F., Carter, C. D., and Hsu, K.-Y., "Characteristics of Cavity-Stabilized Flames in a Supersonic Flow," *Journal of Propulsion and Power*, Vol. 21, No. 4, 2005, pp. 765–768.
doi:10.2514/1.15095
[46] Pitz, R. W., Lahr, M. D., Douglas, Z. W., Wehrmeyer, J. A., Hu, S., Carter, C. D., Hsu, K. Y., Lum, C., and Koochesfahani, M. M., "Hydroxyl Tagging Velocimetry in a Supersonic Flow Over a Cavity," *Applied Optics*, Vol. 44, No. 31, 2005, pp. 6692–6700.
doi:10.1364/AO.44.006692
[47] Gendrich, C. P., and Koochesfahani, M. M., "A Spatial Correlation Technique for Estimating Velocity Fields Using Molecular Tagging Velocimetry (MTV)," *Experiments in Fluids*, Vol. 22, No. 1, 1996, pp. 67–77.
doi:10.1007/BF01893307
[48] Cohn, R. K., and Koochesfahani, M. M., "The Accuracy of Remapping Irregularly Spaced Velocity Data onto a Regular Grid and the Computation of Vorticity," *Experiments in Fluids*, Vol. 29, No. 1, 2000, pp. S61–S69.
doi:10.1007/s003480070008
[49] Pitz, R. W., and Daily, J. W., "Combustion in a Turbulent Mixing Layer Formed at a Rearward-Facing Step," *AIAA Journal*, Vol. 21, No. 11, 1983, pp. 1565–1570.
doi:10.2514/3.8290
[50] Slessor, M. D., Zhuang, M., and Dimotakis, P. E., "Turbulent Shear-Layer Mixing: Growth Rate Compressibility Scaling," *Journal of Fluid Mechanics*, Vol. 414, 2000, pp. 35–45.
doi:10.1017/S0022112099006977

C. Segal
Associate Editor